Методом рентгенівської дифрактометрії досліджено вплив складу двох, трьох, чотирьох і п'яти елементних сплавів на основі ніобію на їх фазово-структурний стан, середній розмір кристалітів і коефіцієнт теплового розширення в інтервалі температур +20…–170 °С. В якості елементів наповнення використовувалися ванадій, тантал, гафній, молібден, цирконій, вольфрам і титан. Ці елементи або в рівноважному – при кімнатній температурі (R_T=+20 °С), або в високотемпературному станах мають ОЦК кристалічну решітку, подібну Nb.

Встановлено, що в сплавах на основі двох, трьох, чотирьох і п'яти елементів для використаних в роботі складів відбувається формування однофазного стану з ОЦК кристалічною решіткою твердого розчину. На структурному рівні вплив складу сплаву позначається на співвідношенні інтенсивностей піків дифракції від різних площин. Для двох порядків дифракції від найбільш щільноупакованної в ОЦК решітці площини {110} виявлено зміну величини інтенсивності для другого порядку дифракції. У найбільшій мірі зменшення відносної інтенсивності відбувається в бінарних сплавах з великою невідповідністю за розмірами атомних радіусів складових компонент. У багатоелементних сплавах спостерігається менше падіння інтенсивності. Це може бути пов'язано зі зменшенням дисторсії кристалічної решітки внаслідок упорядкування елементів, які складають сплав.

На субструктурному рівні склад сплаву позначається на величині середнього розміру кристалітів. Для бінарних складів сплавів найбільший ефект пов'язаний з елементами наповнення Zr і Hf, які мають значно більший атомний радіус. Це призводить до зменшення середнього розміру кристалітів твердого розчину сплаву до найменшого значення 11 нм (сплав NbZr) і виділенню другої фази (сплав NbHf).

Встановлено, що коефіцієнт лінійного теплового розширення (КТР), визначений рентгендифракційним методом при 2-х температурах (RT=+20 °С і Т=–170 °С), в багатоелементних сплавах перевищує значення для вихідних елементів. Найбільше збільшення КТР спостерігається в сплавах, що містять 17–26 ат. % V і W (які мають найменший атомний радіус)

Ключові слова: багатоелементний сплав, ніобій, високоентропійний сплав, дисторсія, фазовий склад, коефіцієнт теплового розширення

UDC 539.261: 669.265
DOI: 10.15587/1729-4061.2020.200264

DETERMINATION OF REGULARITIES OF THE INFLUENCE OF THE ELEMENTAL COMPOSITION OF NIOBIUM-BASED ALLOYS ON THEIR STRUCTURE AND PROPERTIES

O. Sobol`
Doctor of Physical and Mathematical Sciences, Professor*
E-mail: sool@kpi.kharkov.ua
A. Meilekhov
Junior Researcher*
E-mail: meilekhov@gmail.com
V. Subbotina
PhD, Associate Professor*
E-mail: subbotina.valeri@gmail.com
O. Rebrova
PhD, Associate Professor*
E-mail: rebrovaem0512@gmail.com
*Department of Materials Science
National Technical University
"Kharkiv Polytechnic Institute"
Kirpichova str., 2, Kharkiv, Ukraine, 61002

Received date 10.02.2020
Accepted date 30.03.2020
Published date 30.04.2020

1. Introduction

To achieve high functional properties, the main trend in engineering materials science is to obtain materials in conditions far from equilibrium [1, 2]. Moreover, such materials may include a large number of elements (multi-element approach) [3, 4]. Both nonequilibrium production conditions and the multielement approach, in most cases, lead to a significant reduction in the size of crystallite grains and a transition to the nanostructured state [5, 6]. To stabilize this state, for example, the creation of artificial multi-period (multi-layer) composites with nanometer-thick layers is used [7, 8]. Moreover, to obtain high physicomechanical properties, metals with a high heat of formation of interstitial phases are selected as metal components [9, 10].

The same principle is often used to create multi-element alloys with high functional properties [11, 12]. A new direction in the development of multi-element materials was the creation of high-entropy alloys (HEAs), which are a combination of several basic elements (at least five) mixed in approximately equal proportions [13, 14]. High-entropy alloys are defined as alloys consisting of five or more basic elements, each of which should be contained in an amount of 5 to 35 % at [15]. Thus, unlike "classical alloys" having a base element and alloying elements, high-entropy alloys contain a significant number of elements (from 5 or more) introduced in equal or close to equal proportions.

Since all components are mixed in approximately equal proportions, the formation of a matrix based on any one component (as occurs in classical alloys) becomes impossible for HEAs. This leads to a significant difference between

the microstructure and properties of HEAs and traditional alloys [16, 17]. In particular, the use of multi-element alloys with equal proportions of elements allows us to solve the urgent problem of segregation of impurities during radiation exposure, as well as significantly improve the functional properties of the material at high temperatures. In this regard, high-entropy alloys can be considered as promising materials for work in the nodes of the developed high-temperature equipment, as radiation-resistant elements, protective coatings, in the energy sector as elements of machine parts and as hydrogen storage elements.

2. Literature review and problem statement

In [18, 19], the results of determining the phase composition of high-entropy alloys are presented. It has been shown that in HEAs (as in alloys having a large number of basic elements and high entropy of mixing), the formation of solid solutions is preferable from the thermodynamic point of view. It was found [20, 21] that high-entropy alloys consisting of transition metals are prone to the formation of a single-phase state of a solid solution with a relatively simple crystal lattice (bcc, fcc, hcp). However, the problem of selecting elements to create a structural state of uniform volume in such materials remains unresolved.

It was substantiated in [22, 23] that during the formation of high-entropy alloys based on solid solutions with simple crystal lattices, several effects should be expected: High Entropy Effect, Lattice Distortion Effect, Cocktail Effect. The High Entropy Effect lies in the fact that the higher entropy of mixing (mainly configurational) in HEAs reduces the free energy of the phases of the solid solution and facilitates their formation, especially at higher temperatures. The Lattice Distortion Effect is due to different atomic radii of the elements and leads to a change in the principle of motion of dislocations, and the Cocktail Effect leads to a change in the properties of the alloy compared to the properties of its constituent elements. However, theoretical models of these effects require experimental verification for different types of alloys.

As a result of these effects, high functional characteristics of HEAs can be achieved [24]. First of all, it is the high strength of these alloys in the cast and annealed states (700–2,600 MPa) [25, 26]. In addition to high strength, high-entropy alloys are characterized by high hardness [27] and high wear resistance [28, 29]. Also, these alloys are not inferior to corrosion-resistant steels in their anti-corrosion properties [30, 31]. However, a logical study of the relationship between the obtained properties and the structural state of alloys was practically not carried out in these works.

It was assumed in [32, 33] that in many respects the uniqueness of the properties of high-entropy alloys is determined by the distortion of the crystal lattice. Low diffusion mobility, which leads to a stable state of crystal lattices of high symmetry, high hardness, and high resistance to radiation influences, is also associated with this [34, 35]. In this case, the practical determination of lattice distortion in multielement alloys of various types remains a problem.

Theoretically, the δ parameter is commonly used to quantify distortion (lattice distortion). It represents the deviation of the metal radii of the elements from the average radius [36]:

$$\delta = \sqrt{\sum_{i=1}^{n} c_i \left(1 - \frac{r_i}{\overline{r}}\right)^2},$$

where c_i is the atomic percentage of the i-th element, r_i and r are the radius of the atom and the average atomic radius:

$$\overline{r} = \sum_{i=1}^{N} c_i r_i.$$

Moreover, the dependence of the δ parameter on the composition for different elements has the form of a continuous function. However, it can be assumed that with a larger difference in the atomic radii of closely spaced atoms, concentration points of bifurcation may appear. In this case, the continuous nature of this dependence will be violated and qualitative changes in the structure, phase composition, and properties of the alloy may occur.

In this regard, it should be noted that the formation of precipitates with a different type of crystal lattice (compared with the base) at low annealing temperatures (about 600 °C [37, 38]) is a new direction in hardening high-entropy alloys. Note that this can be an indirect confirmation of the presence of clusters of atoms with a small difference in radii already at the stage of alloy formation.

Thus, the analysis of published data indicates that, despite the large number of works on high-entropy alloys, structural engineering of this type of material is a very difficult task. The presence of different structural models for enhancing the functional properties of high-entropy alloys makes it necessary to determine experimental relationships between the properties of HEA alloys and their elemental composition and structural state.

3. The aim and objectives of the study

The aim of the study is to determine patterns of influence of the elemental composition of niobium-based alloys on their phase-structural state, crystallite size and coefficient of linear thermal expansion in the temperature range +20...–170 °C.

To achieve the aim, the following objectives were set:

– to study the effect of the elemental composition of two, three, four and five elemental niobium-based alloys on their phase-structural state and determine the patterns of influence of the composition of alloys on the average crystallite size;

– to find the dependence of the coefficient of linear thermal expansion in multi-element alloys on their composition.

4. Methodology for the synthesis of high-entropy alloys and methods of investigation

In the preparation of alloys, vanadium, tantalum, hafnium, molybdenum, zirconium, tungsten and titanium were used as filling elements for niobium (as the basic element of all alloys). These elements either in equilibrium – at room temperature (R_T=+20 °C), or in high-temperature states have a bcc crystal lattice similar to Nb. Also, the choice of these elements as components of a high-entropy alloy was due to their different atomic radii. Thus, the elements V, W, and Mo have a significantly smaller atomic radius compared to Nb. The atomic radii of Zr and Hf significantly exceed the

atomic radius of Nb, and Ta and Ti have an atomic radius close to Nb.

Ingots of high-entropy alloys were produced by vacuum-arc melting in an atmosphere of high-purity argon [39]. Melting was carried out with a non-consumable tungsten electrode in a copper water-cooled hearth. To homogenize the composition, the obtained ingots were remelted 6–7 times with a cooling rate of about 50 K/s.

X-ray diffraction studies of the samples were carried out on DRON-3M and DRON-4 diffractometers (IC Burevestnik, Russia) in Cu–K_α radiation when scattering was recorded in a discrete recording mode with a graphite monochromator on a secondary beam [40]. The scanning step varied within $\Delta(2\vartheta)=0.01...0.05^\circ$ (depending on the half-width and intensity of diffraction peaks). Depending on the intensity of diffraction peaks, the exposure time at a point of 40 or 100 s was used when recording the spectra.

The crystallite size was determined by approximating the shape of the diffraction peaks for two diffraction orders in the direction of the selected axis [41]. Two diffraction orders in the direction of the [110] axis were used in the work. To achieve high accuracy, the diffraction reflexes were taken in the exposure mode for 100 seconds at a point with a scan step of 0.05°.

Low-temperature studies (up to –170 °C) were carried out using the modernized URNT-180 low-temperature chamber. Low-temperature studies made it possible to exclude the influence of chemical reactions in determining the coefficient of temperature linear expansion. Also, the determination of the KTE value at low temperatures made it possible to exclude the influence of the ordering processes that are characteristic of multi-element alloys at high temperatures. At the same time, the choice of the temperature range of –170...+20 °C is due to the technological capabilities of the URNT-180 chamber.

Fig. 1 shows a general view of the "DRON-3M diffractometer – URNT-180 low-temperature chamber" complex. For comparative studies, the diffraction curves obtained at a low temperature on the sample (about –170 °C) were compared with the diffraction curves obtained at room temperature (R_T=+20 °C).

Fig. 1. General view of the "DRON-3M diffractometer – URNT-180 low-temperature chamber" complex

To study the elemental composition, the X-ray fluorescence method was used. An SPRUT-2 X-ray fluorescence spectrometer (Joint-Stock Company "Ukrentgen", Ukraine) was used as a basic setup [42]. As the primary (exciting) radiation, we used the radiation of an X-ray tube with an Ag anode at a voltage of 42 kV.

5. Results of research of the influence of the elemental composition on the phase-structural state of Nb-based alloys

For determining the distortion, clustering, and other structural parameters, as well as optimizing the elemental composition to obtain the required properties, it is necessary to take into account the influence of each element. In multi-element alloys, the available experimental methods make this very difficult (almost impossible). In this regard, in this work, we used an approach to find regularities with a gradual increase in the number of constituent elements in the alloy. Nb was chosen as the basic element (i.e., the element included in all the studied alloys). The choice of niobium is due to the fact that this element has good physical and mechanical characteristics, however, it was practically not used in high-entropy alloys.

Using Nb as the base material, the alloys were studied in the work, the filling of which with elements varied from two to five. The elemental composition after the fusion process was determined by the method of X-ray fluorescence analysis [42]. The results of the elemental compositions of the alloys are given in Table 1.

Table 1

Elemental composition of alloys

Series number	C at,%							
	Nb	V	W	Mo	Zr	Ta	Ti	Hf
1	85.93	14.07	0	0	0	0	0	0
2	83.59	0	16.41	0	0	0	0	0
3	73.51	0	0	0	26.49	0	0	0
4	82.55	0	0	0	0	17.45	0	0
5	83.43	0	0	0	0	0	16.57	0
6	74.17	0	0	0	0	20.81	5.02	0
7	79.45	0	0	0	0.44	0	0	20.11
8	54.45	23.10	22.45	0	0	0	0	0
9	53.36	22.65	0	0	0	23.99	0	0
10	30.39	26.45	20.15	0.13	0	22.88	0	0
11	42.54	0	18.72	19.82	0	18.92	0	0
12	22.77	17.13	18.19	0	23.13	18.78	0	0
13	24.48	12.82	20.75	20.79	0	21.16	0	0
14	27.02	11.35	0	0	20.16	21.24	20.23	0

In accordance with the classical material science triad (composition, structure, properties), the second important characteristic of materials is their phase-structural state.

In this work, to study the phase-structural state, the method of x-ray diffractometry was used. The resulting diffraction spectra for each of the series of alloys are shown in Fig. 2, 3.

Fig. 2 shows the spectra for two-element alloys based on Nb. It can be seen that in the Nb-Ti and Nb-Ta alloys (based on elements with a small difference in atomic radii), a single-phase state (bcc lattice) is formed without revealing

diffraction peaks from planes of other phases. Note that this system is characterized by a relatively large crystallite size of 18 nm and 30 nm, respectively.

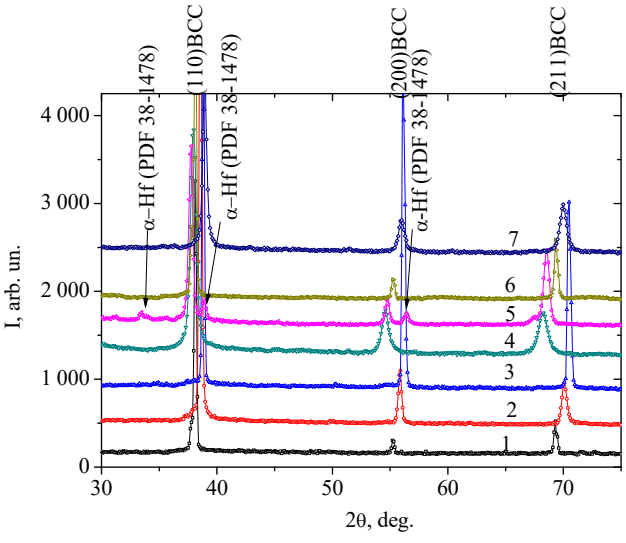

Fig. 2. XRD patterns for niobium (1), as well as XRD patterns for two-component alloys based on it: 2 — NbW (series 2 in Table 1), 3 — NbV (series 1 in Table 1), 4 — NbZr (series 3 in Table 1), 5 — NbHf (series 7 in Table 1), 6 — NbTa (series 4 in Table 1), 7 — NbTi (series 5 in Table 1)

Also, diffraction peaks from other phases are not detected for the Nb-V and Nb-W systems, where the doping elements (V and W) have a smaller atomic radius than Nb [43]. The crystallite size for these systems is also relatively large 20–29 nm.

At the structural level, in all the alloys obtained, the preferred orientation of crystallites with the [110] axis is formed. This is manifested in the diffraction spectra by increasing the relative intensity of the diffraction peak from the (110) plane. However, the second-order intensity of diffraction from the (220) plane (due to the low intensity of the survey of peaks (220) was carried out separately from the main spectrum) largely depends on the alloy composition. Table 2 shows the generalized values of the $I_{(110)}/I_{(220)}$ ratio for all types of alloys.

Table 2

Value of the ratio of the integrated intensity of the peaks $I_{(110)}/I_{(220)}$ for alloys of different elemental compositions

Sample number in accordance with Table 1	1	2	3	4	5	6	7	8	9	10	11	12	13	14
$I_{(110)}/I_{(220)}$	35	31	32	21	5	18	21	21	8	8	19	16	16	20

Data from Table 2 show the nonmonotonic character of the $I_{(110)}/I_{(220)}$ value from the alloy compositions. It can be seen that the largest ratio $I_{(110)}/I_{(220)}$ is inherent in binary alloys, which consist of elements with very different atomic radii (NbV, NbW and NbZr). Such a large decrease in intensity for the second order of reflection (from the plane (220)) indicates a large distortion of the crystal lattice in this case. At the same time, in multi-element alloys, the of $I_{(110)}/I_{(220)}$ value is somewhat lower. The reason for this effect may be a partial relaxation of the deformation factor during cluster formation in multielement alloys.

For alloys consisting of 3 or more elements (Fig. 3), the main phase is also a solid solution based on a bcc crystal lattice. However, multielement alloys are characterized by asymmetry of the diffraction line profiles associated with the heterogeneity of the solid solution over the volume of the samples.

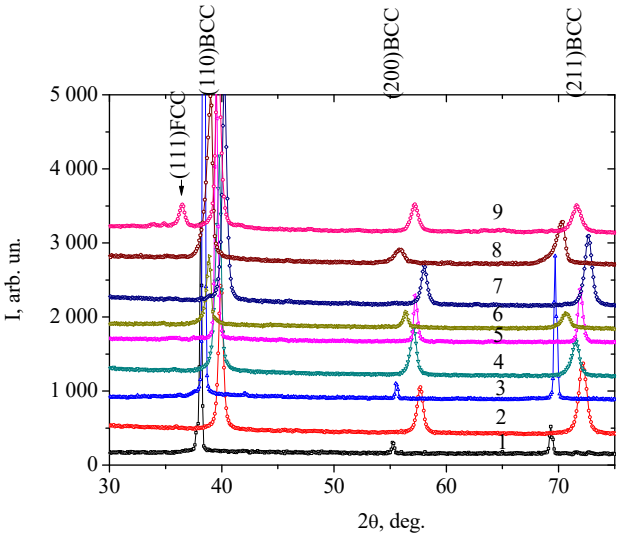

Fig. 3. XRD patterns for niobium (1), as well as XRD patterns for multicomponent alloys based on it: 2 — NbVW (series 8 in Table 1), 3 — NbTaTi (series 6 in Table 1), 4 — NbVTa (series 9 in Table 1), 5 — NbVWTa (series 10 in Table 1), 6 — NbWTaMo (series 11 in Table 1), 7 — NbVWTaMo (series 13 in Table 1), 8 — NbVZrTaTi (series 14 in table 1), 9 — NbVWTaZr (series 12 in Table 1)

The appearance of the second system of diffraction peaks inherent in the fcc lattice (Fig. 3, spectrum 9) was also noted for the 12 series alloy. Moreover, if we relate the decrease in crystallite size in these alloys with the influence of crystal lattice deformation, then the formation of the NbTaTi alloy (series 6) and NbWVTa (series 10) leads to the least deformation. For these alloys, the crystallite size estimated from the width of the diffraction reflections is 31 nm and 27 nm, respectively. In this case, the average crystallite size in pure Nb is about 45 nm.

However, the smallest crystallite size (in comparison with 3- and 4-element alloys) is inherent in five-element alloys. This can be an indirect confirmation of the large lattice deformation in these alloys, which stimulates dispersion with strain relaxation at the formed intergranular interfaces. Accordingly, for the NbWVTaMo (series 13, spectrum 7), NbVZrTaTi (series 14, spectrum 8) and NbWVTaZr (series 12, spectrum 9) alloys, the average crystallite size is 13.3 nm, 14.4 nm, and 11.7 nm.

6. Results of research of the influence of the elemental composition of Nb-based alloys on their coefficient of thermal linear expansion

A physical property that can be determined by structural changes at different temperatures is the thermal

expansion coefficient (CTE) of the alloy. To determine it from the data of diffraction spectra, we used the technique previously described in detail in [44]. Comparison of diffraction spectra was carried out for two temperature regimes: at room temperature (R_T=+20°C) and low temperature near –170 °C (close to the boiling point of liquid nitrogen –195.75 °C). The calculation was carried out based on the shift of the diffraction peak from the (321) plane of the bcc crystal lattice of the solid solution, which is the optimal recording mode in Cu–K_α radiation, based on studies [44].

Table 3 shows the values of the coefficient of thermal expansion (CTE, α) for alloys of different compositions. For the remaining alloys, the determination of the coefficient of thermal expansion by the shift of the peak at large diffraction angles from the (321) plane did not allow strong smearing of the diffraction peaks (321) and the presence of asymmetry due to inhomogeneous solid solutions (Fig. 4).

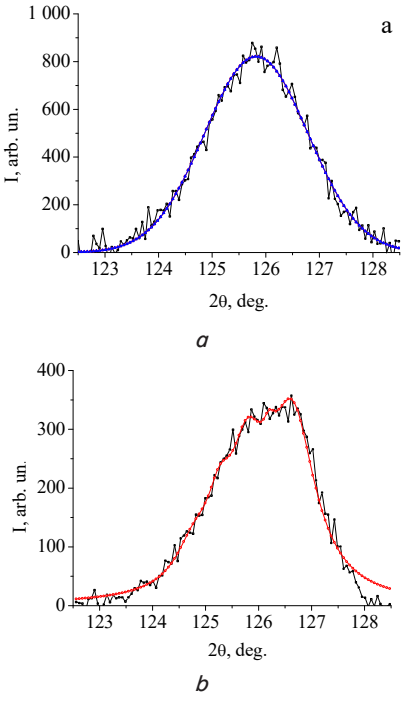

Fig. 4. XRD peak (321): *a* — alloy of series 13 with a homogeneous solid solution, *b* — alloy of series 6 with smearing of the diffraction peak due to superposition of spectra from inhomogeneous solid solutions

For Nb, the obtained value of $\alpha_{Nb}=0.46\cdot10^{-5}$ K^{-1} corresponds to the standard value of the CTE of niobium in the bulk state [44].

A comparison of the obtained values for alloys of other compositions (Table 3) shows that the introduction of Zr (series 3) does not lead to a significant increase in the CTE of the niobium base. Also, doping with elements such as Ti and Mo (series 13 and 14) does not lead to a significant increase in the CTE.

Table 3

Coefficient of thermal expansion (α) for alloys of different elemental compositions

Sample number in accordance with Table 1	Nb	1	3	8	9	10	11	12	13	14
α, 10^{-5}, K^{-1}	0.46	0.76	0.53	1.24	0.93	1.64	0.97	1.59	0.82	0.72

In contrast to these elements, the introduction of vanadium (series 1), and especially the combination of V+W (series 8 and 10), leads to a more than 3-fold increase in CTE. Moreover, in pure form, for example, for W, the CTE is much lower than for Nb ($\alpha_W=0.436\cdot10^{-5}$ K^{-1} [45]). It can be assumed that the increase in the thermal expansion coefficient when creating an alloy of this element with niobium is associated with a significantly smaller atomic radius of W (and even more V) compared to the atomic radius of the base Nb [43]. In this regard, in the Nb–V alloy, the small atomic radius of vanadium can also be considered as the main factor in the increase in the CTE.

7. Discussion of the alloys elemental composition effects on their phase-structural state and CTE

The mismatch between the atomic radii of the elements making up the solid solution significantly affects the phase-structural state and properties.

For the niobium-based alloys studied in this work, at the phase-structural level, the greatest effect is associated with the content of atoms with a large atomic radius (Hf and Zr). As can be seen from Fig. 2, in the Nb-Hf alloy, the large difference in atomic radii (9 %) is apparently critical. For this alloy, peaks are observed in the diffraction spectra, both inherent in the planes of the bcc lattice, and for the α-Hf phase (PDf 38-1478) with a non-cubic type of crystal lattice (spectra 5 in Fig. 2). The driving force for the formation of the second phase, apparently, is the large deformation of the crystal lattice at a high concentration of impurity atoms with a large discrepancy in atomic radii. As a result of this, the displacement of a part of impurity atoms to the crystallite boundaries and the formation of a new phase based on impurity elements (in this case, Hf) become thermodynamically beneficial. The formation of such a phase is accompanied by the accumulation of a significant part of impurity atoms in it, which accordingly leads to their lower content in the basic bcc Nb lattice. As an estimate based on the Vegard rule showed, in the Nb–Hf alloy, the dissolution of Hf in the bcc Nb lattice is about 6.5 % (with a total Hf content in the alloy of 20.11 at. %). Such a relatively small percentage of dissolved atoms does not lead to a critically large deformation of the crystal lattice. The absence of a critical strain value allows one to achieve large average crystallite sizes, which is observed experimentally (the average crystallite size of the bcc lattice in the Nb–Hf system is 18 nm).

The Nb-Zr alloy should be considered separately. In this alloy, the formation of a single-phase state occurs at a large difference in atomic radii (11 %). In this case, microdeformation of the lattice due to the large discrepancy leads to strong crushing of crystallites, the average value of which is the smallest among all alloy systems and is 11 nm.

The dispersion effect also becomes significant in five-element (high-entropy) alloys. In this case, apparently, a large content of atoms of different elements impedes their mobility and limits the growth areas of crystallites. This is especially evident in the NbWVTaZr alloy, which contains atoms with very different atomic radii (with small – W and V, with large – Zr).

The noted structural features of the alloys also affect their properties.

As can be seen from the results of determining the coefficient of thermal linear expan-

sion (Table 3), in this case, the critical elements that allow to increase the thermal expansion coefficient are elements with a relatively small atomic radius (W and V). During the formation of such alloys, the presence in the crystal lattice of disordered atoms with a significantly smaller atomic radius leads to a weakening of the bond at the lattice sites and thus contributes to an increase in the amplitude of atomic vibrations during thermal exposure.

The results obtained in this work can be used to develop multi-element materials based on Nb in a single-phase state with the necessary structural state and properties. In the future, it is planned to conduct studies on other types of multi-element alloys (with basic elements Ti and Mo) in order to find a generalized material science criterion for selecting the elemental composition to achieve the necessary functional properties in these alloys.

8. Conclusions

1. The influence of the elemental composition of niobium-based alloys with a bcc crystal lattice using elements having a modification with a similar bcc crystal lattice was studied. It is found that in alloys with the content of 2, 3, 4 and 5 elements, a single-phase state is formed with a bcc crystal lattice of a solid solution. At the substructural level, the alloy composition affects the average crystallite size. In the formation of Nb-based binary alloys with elements having a close (Ta, Ti) or significantly smaller (V, W) atomic radius, the average crystallite size of the alloy is in the range of 18–30 nm. The formation of Nb-based binary alloys with Zr and Hf elements having a significantly larger atomic radius leads to a decrease in the average crystallite size of the alloy solid solution to 11 nm (NbZr alloy) and the precipitation of the second phase (NbHf alloy).

For all types of 3- and 4-element alloys studied in the work, the average crystallite size is relatively large and amounted to 25–30 nm. In alloys containing 5 elements, the crystallite size does not exceed 15 nm, and the lowest value (11.7 nm) was found for the NbWVTaZr alloy.

2. It is found that the coefficient of linear thermal expansion, determined by the X-ray diffraction method in the temperature range of +20°C...–170 °C, in multi-element alloys exceeds the values for the starting elements. The largest increase in CTE is observed in alloys containing 17–26 at. % V and W, which have the smallest atomic radius.

Acknowledgments

The authors are grateful to the Academician of the NAS of Ukraine S. A. Firstov, Doctor of Technical Sciences V. F. Gorban and PhD N. A. Krapivko for the provided samples for research and STCU Foundation (project 6360 “New high temperature materials based on the multicomponent (high-entropy) alloys with controlled nanoclustered structure”) for financial support.

References

1. Mayrhofer, P. H., Mitterer, C., Hultman, L., Clemens, H. (2006). Microstructural design of hard coatings. Progress in Materials Science, 51 (8), 1032–1114. doi: https://doi.org/10.1016/j.pmatsci.2006.02.002
2. Sobol, O. V., Postelnyk, A. A., Meylekhov, A. A., Andreev, A. A., Stolbovoy, V. A. (2017). Structural Engineering of the Multilayer Vacuum Arc Nitride Coatings Based on Ti, Cr, Mo and Zr. Journal of Nano- and Electronic Physics, 9 (3), 03003-1–03003-6. doi: https://doi.org/10.21272/jnep.9(3).03003
3. Azarenkov, N. A., Sobol', O. V., Beresnev, V. M., Pogrebnyak, A. D., Kolesnikov, D. A., Turbin, P. V., Toryanik, I. N. (2013). Vacuum-plasma coatings based on the multielement nitrides. Metallofizika i noveishie tekhnologii, 35 (8), 1061–1084. Available at: http://dspace.nbuv.gov.ua/bitstream/handle/123456789/104178/07-Azarenkov.pdf?sequence=1
4. Cherepova, T., Dmitrieva, G., Tisov, O., Dukhota, O., Kindrachuk, M. (2019). Research on the Properties of Co-Tic and Ni-Tic Hip-Sintered Alloys. Acta Mechanica et Automatica, 13 (1), 57–67. doi: https://doi.org/10.2478/ama-2019-0009
5. Sobol', O. V., Andreev, A. A., Stolbovoi, V. A., Fil'chikov, V. E. (2012). Structural-phase and stressed state of vacuum-arc-deposited nanostructural Mo-N coatings controlled by substrate bias during deposition. Technical Physics Letters, 38 (2), 168–171. doi: https://doi.org/10.1134/s1063785012020307
6. Sobol', O. V., Andreev, A. A., Gorban', V. F., Krapivka, N. A., Stolbovoi, V. A., Serdyuk, I. V., Fil'chikov, V. E. (2012). Reproducibility of the single-phase structural state of the multielement high-entropy Ti-V-Zr-Nb-Hf system and related superhard nitrides formed by the vacuum-arc method. Technical Physics Letters, 38 (7), 616–619. doi: https://doi.org/10.1134/s1063785012070127
7. Sobol', O. V., Andreev, A. A., Gorban', V. F., Meylekhov, A. A., Postelnyk, H. O. (2016). Structural Engineering of the Vacuum Arc ZrN/CrN Multilayer Coatings. Journal of Nano- and Electronic Physics, 8 (1), 01042-1–01042-5. doi: https://doi.org/10.21272/jnep.8(1).01042
8. Sobol', O. V., Andreev, A. A., Gorban', V. F., Stolbovoy, V. A., Melekhov, A. A., Postelnyk, A. A. (2016). Possibilities of structural engineering in multilayer vacuum-arc ZrN/CrN coatings by varying the nanolayer thickness and application of a bias potential. Technical Physics, 61 (7), 1060–1063. doi: https://doi.org/10.1134/s1063784216070252
9. Sobol', O. V., Meilekhov, A. A. (2018). Conditions of Attaining a Superhard State at a Critical Thickness of Nanolayers in Multiperiodic Vacuum-Arc Plasma Deposited Nitride Coatings. Technical Physics Letters, 44 (1), 63–66. doi: https://doi.org/10.1134/s1063785018010224
10. Sobol', O. V., Andreev, A. A., Gorban', V. F. (2016). Structural Engineering of Vacuum-ARC Multiperiod Coatings. Metal Science and Heat Treatment, 58 (1-2), 37–39. doi: https://doi.org/10.1007/s11041-016-9961-3

11. Raghavan, R., Hari Kumar, K. C., Murty, B. S. (2012). Analysis of phase formation in multi-component alloys. Journal of Alloys and Compounds, 544, 152–158. doi: https://doi.org/10.1016/j.jallcom.2012.07.105
12. Senkov, O. N., Wilks, G. B., Scott, J. M., Miracle, D. B. (2011). Mechanical properties of Nb25Mo25Ta25W25 and V20Nb20Mo20Ta20W20 refractory high entropy alloys. Intermetallics, 19 (5), 698–706. doi: https://doi.org/10.1016/j.intermet.2011.01.004
13. Ranganathan, S. (2003). Alloyed pleasures: multimetallic cocktails. Current science, 85 (10), 1404–1406. Available at: https://pdfs.semanticscholar.org/e4d2/1223b04a774d2ac1b134bb46cfc0ba810f43.pdf
14. Li, C., Li, J. C., Zhao, M., Jiang, Q. (2009). Effect of alloying elements on microstructure and properties of multiprincipal elements high-entropy alloys. Journal of Alloys and Compounds, 475 (1-2), 752–757. doi: https://doi.org/10.1016/j.jallcom.2008.07.124
15. Sobol', O. V., Yakushchenko, I. V. (2015). Influence of ion implantation on the structural and stressed state and mechanical properties of nitrides of high-entropy (TiZrAlYNb)N and (TiZrHfVNbTa)N alloys. Journal of nano- and electronic physics, 7 (3), 03044-1-03044-6. Available at: http://jnep.sumdu.edu.ua/download/numbers/2015/3/articles/jnep_2015_V7_03044.pdf
16. Yeh, J.-W., Chen, S.-K., Lin, S.-J., Gan, J.-Y., Chin, T.-S., Shun, T.-T. et. al. (2004). Nanostructured High-Entropy Alloys with Multiple Principal Elements: Novel Alloy Design Concepts and Outcomes. Advanced Engineering Materials, 6 (5), 299–303. doi: https://doi.org/10.1002/adem.200300567
17. Sobol', O. V., Andreev, A. A., Gorban', V. F., Postelnyk, H. O., Stolbovoy, V. A., Zvyagolsky, A. V. et. al. (2019). The use of negative bias potential for structural engineering of vacuum-arc nitride coatings based on high-entropy alloys. Problems of atomic science and technology, 120 (2), 127–135. Available at: https://vant.kipt.kharkov.ua/ARTICLE/VANT_2019_2/article_2019_2_127.pdf
18. Guo, S., Liu, C. T. (2011). Phase stability in high entropy alloys: Formation of solid-solution phase or amorphous phase. Progress in Natural Science: Materials International, 21 (6), 433–446. doi: https://doi.org/10.1016/s1002-0071(12)60080-x
19. Zhang, Y., Zhou, Y. J., Lin, J. P., Chen, G. L., Liaw, P. K. (2008). Solid-Solution Phase Formation Rules for Multi-component Alloys. Advanced Engineering Materials, 10 (6), 534–538. doi: https://doi.org/10.1002/adem.200700240
20. Pickering, E. J., Jones, N. G. (2016). High-entropy alloys: a critical assessment of their founding principles and future prospects. International Materials Reviews, 61 (3), 183–202. doi: https://doi.org/10.1080/09506608.2016.1180020
21. Cantor, B., Chang, I. T. H., Knight, P., Vincent, A. J. B. (2004). Microstructural development in equiatomic multicomponent alloys. Materials Science and Engineering: A, 375-377, 213–218. doi: https://doi.org/10.1016/j.msea.2003.10.257
22. Chen, J., Zhou, X., Wang, W., Liu, B., Lv, Y., Yang, W. et. al. (2018). A review on fundamental of high entropy alloys with promising high–temperature properties. Journal of Alloys and Compounds, 760, 15–30. doi: https://doi.org/10.1016/j.jallcom.2018.05.067
23. Cheng, C.-Y., Yang, Y.-C., Zhong, Y.-Z., Chen, Y.-Y., Hsu, T., Yeh, J.-W. (2017). Physical metallurgy of concentrated solid solutions from low-entropy to high-entropy alloys. Current Opinion in Solid State and Materials Science, 21 (6), 299–311. doi: https://doi.org/10.1016/j.cossms.2017.09.002
24. Miracle, D. B., Senkov, O. N. (2017). A critical review of high entropy alloys and related concepts. Acta Materialia, 122, 448–511. doi: https://doi.org/10.1016/j.actamat.2016.08.081
25. Zhang, Y., Yang, X., Liaw, P. K. (2012). Alloy Design and Properties Optimization of High-Entropy Alloys. JOM, 64 (7), 830–838. doi: https://doi.org/10.1007/s11837-012-0366-5
26. Florea, I., Florea, R. M., Baltatescu, O., Soare, V., Chelariu, R., Carcea, I. (2013). High entropy alloys. Journal of Optoelectronics and Advanced Materials, 15 (7-8), 761–767. Available at: https://www.researchgate.net/publication/274640494_High_entropy_alloys
27. Tang, W.-Y., Yeh, J.-W. (2009). Effect of Aluminum Content on Plasma-Nitrided Al x CoCrCuFeNi High-Entropy Alloys. Metallurgical and Materials Transactions A, 40 (6), 1479–1486. doi: https://doi.org/10.1007/s11661-009-9821-5
28. Chen, M.-R., Lin, S.-J., Yeh, J.-W., Chen, S.-K., Huang, Y.-S., Tu, C.-P. (2006). Microstructure and Properties of Al0.5CoCrCuFeNiTix (x=0–2.0) High-Entropy Alloys. Materials Transactions, 47 (5), 1395–1401. doi: https://doi.org/10.2320/matertrans.47.1395
29. Wu, J.-M., Lin, S.-J., Yeh, J.-W., Chen, S.-K., Huang, Y.-S., Chen, H.-C. (2006). Adhesive wear behavior of AlxCoCrCuFeNi high-entropy alloys as a function of aluminum content. Wear, 261 (5-6), 513–519. doi: https://doi.org/10.1016/j.wear.2005.12.008
30. Chen, Y. Y., Hong, U. T., Shih, H. C., Yeh, J. W., Duval, T. (2005). Electrochemical kinetics of the high entropy alloys in aqueous environments – a comparison with type 304 stainless steel. Corrosion Science, 47 (11), 2679–2699. doi: https://doi.org/10.1016/j.corsci.2004.09.026
31. Chen, Y. Y., Duval, T., Hung, U. D., Yeh, J. W., Shih, H. C. (2005). Microstructure and electrochemical properties of high entropy alloys – a comparison with type-304 stainless steel. Corrosion Science, 47 (9), 2257–2279. doi: https://doi.org/10.1016/j.corsci.2004.11.008
32. Wang, Z., Fang, Q., Li, J., Liu, B., Liu, Y. (2018). Effect of lattice distortion on solid solution strengthening of BCC high-entropy alloys. Journal of Materials Science & Technology, 34 (2), 349–354. doi: https://doi.org/10.1016/j.jmst.2017.07.013

33. Tong, C.-J., Chen, Y.-L., Yeh, J.-W., Lin, S.-J., Chen, S.-K., Shun, T.-T. et. al. (2005). Microstructure characterization of Al x CoCrCuFeNi high-entropy alloy system with multiprincipal elements. Metallurgical and Materials Transactions A, 36 (4), 881–893. doi: https://doi.org/10.1007/s11661-005-0283-0
34. Andreev, A. A., Voyevodin, V. N., Sobol', O. V., Gorban', V. F., Kartmazov, G. N., Stolbovoy, V. A. et. al. (2013). Regularities in the effect of model ion irradiation on the structure and properties of vacuum-arc nitride coatings. Problems of atomic science and technology, 5 (87), 142–146. Available at: https://vant.kipt.kharkov.ua/ARTICLE/VANT_2013_5/article_2013_5_142.pdf
35. Sobol', O. V., Dur, O., Postelnyk, A. A., Kraievska, Z. V. (2019). Structural engineering and functional properties of vacuum-arc coatings of high-entropy (TiZrNbVHf)N and (TiZrNbVHfTa)N alloys nitrides. Functional materials, 26 (2), 310–318. doi: https://doi.org/10.15407/fm26.02.310
36. Yeh, J.-W. (2013). Alloy Design Strategies and Future Trends in High-Entropy Alloys. JOM, 65 (12), 1759–1771. doi: https://doi.org/10.1007/s11837-013-0761-6
37. Stepanov, N. D., Shaysultanov, D. G., Ozerov, M. S., Zherebtsov, S. V., Salishchev, G. A. (2016). Second phase formation in the CoCrFeNiMn high entropy alloy after recrystallization annealing. Materials Letters, 185, 1–4. doi: https://doi.org/10.1016/j.matlet.2016.08.088
38. Stepanov, N. D., Yurchenko, N. Y., Zherebtsov, S. V., Tikhonovsky, M. A., Salishchev, G. A. (2018). Aging behavior of the HfNbTaTiZr high entropy alloy. Materials Letters, 211, 87–90. doi: https://doi.org/10.1016/j.matlet.2017.09.094
39. Firstov, S. A., Gorban', V. F., Krapivka, N. A., Pechkovskiy, E. P. (2012). Raspredelenie elementov v lityh mnogokomponentnyh vysokoentropiynyh odnofaznyh splavah s OTSK kristallicheskoy reshetkoy. Kompozity i nanomaterialy, 3, 48–65.
40. Sobol', O. V., Shovkoplyas, O. A. (2013). On advantages of X-ray schemes with orthogonal diffraction vectors for studying the structural state of ion-plasma coatings. Technical Physics Letters, 39 (6), 536–539. doi: https://doi.org/10.1134/s1063785013060126
41. Jenkins, R., Snyder, R. L. (1996). Introduction to X-ray Powder Diffractometry. John Wiley & Sons Inc. doi: https://doi.org/10.1002/9781118520994
42. Mikhailov, I. F., Baturin, A. A., Mikhailov, A. I., Borisova, S. S. (2012). Increasing the sensitivity of X-ray fluorescent scheme with secondary radiator using the initial spectrum filtration. Functional materials, 19 (1), 126–129. Available at: http://dspace.nbuv.gov.ua/bitstream/handle/123456789/135279/21-Mikhailov.pdf?sequence=1
43. Heyrovska, R. (2013). Atomic, ionic and bohr radii linked via the golden ratio for elements of groups 1 - 8 including lanthanides and actinides. International journal of sciences, 2, 63–68. Available at: https://www.ijsciences.com/pub/pdf/V2-201304-18.pdf
44. Finkel', V. A. (1971). Nizkotemperaturnaya rentgenografiya metallov. Moscow: Metallurgiya, 256.
45. Chirkin, V. S. (1967). Teplofizicheskie svoystva materialov yadernoy tehniki. Moscow: Atomizdat, 474.